Crystal Nucleation and Growth in Poly(ethylene terephthalate)/Alumina-Nanoparticle Composites

Praveen Bhimaraj,[1,2]* Hoichang Yang,[1] Richard W. Siegel,[1,2] Linda S. Schadler[1,2]

[1]*Rensselaer Nanotechnology Center, Rensselaer Polytechnic Institute, Troy, New York 12180*
[2]*Department of Materials Science and Engineering, School of Engineering, Rensselaer Polytechnic Institute, Troy, New York 12180*

Received 16 October 2006; accepted 26 June 2007
DOI 10.1002/app.27097
Published online 7 September 2007 in Wiley InterScience (www.interscience.wiley.com).

ABSTRACT: The effect of nanoparticles on nonisothermal polymer crystallization was investigated using poly(ethylene terephthalate) (PET) nanocomposites with alumina (Al_2O_3) nanoparticles of average size 38 nm. The filler content in the nanocomposites was varied from 0 to 10 wt %. The interparticle spacing was observed to decrease (as expected) with an increase in loading of the nanoparticles. Contrary to previous reports in the literature on semicrystalline polymer-based composites with micron-size and macroscale particles, our differential scanning calorimetry, transmission electron microscopy, and X-ray studies showed that the addition of the nanoparticles did not cause heterogeneous nucleation of PET crystals in nanocomposites containing up to 3 wt % Al_2O_3. This is attributed to the nanoparticle curvature being comparable to the radius of gyration of the polymer. The addition of the nanoparticles was found to disrupt the spherulitic morphology of the PET because of their physical presence and their proximity to one another. © 2007 Wiley Periodicals, Inc. J Appl Polym Sci 106: 4233–4240, 2007

Key words: polyester; nanoparticle; alumina; nanocomposite; heterogeneous nucleation

INTRODUCTION

The crystallization of semicrystalline polymers is an area of interesting and intriguing research. Part of the intrigue is due to the different levels of crystal structure that exist in semicrystalline polymers.[1–3] Macromolecules fold to develop a crystal unit-cell structure during crystallization. The folding continues to form crystalline lamellae. Several lamellae grow radially outward from a single nucleus into a spherulite until they impinge with adjacent spherulites.

The incorporation of fillers is known to affect both the crystal nucleation and growth of semicrystalline polymer matrices. From a thermodynamics perspective, the presence of a high-energy inorganic surface (e.g., inorganic fillers) promotes heterogeneous crystal nucleation of polymers.[4] Also, a low surface-energy filler can act as an ineffective nucleation site.[5] While some studies have shown that the loading of nanofillers promotes the crystal nucleation of a polymer matrix,[6,7] filler-induced crystals have been observed to occur from relatively planar filler surfaces.[8–10] When the nanofiller surface curvature becomes comparable to the radius of gyration (R_g) of the polymer, it is still an open question whether the fillers will promote crystal nucleation.[11] The presence of nanofillers can also affect other levels of the polymer crystal hierarchy (such as lamellae thickness or spherulite organization).[12–14] Furthermore, the presence of the fillers can hinder the growth of the crystals, depending on the change in geometrical interparticle spacing.[15]

In this article, we explore the crystallization behavior of the matrix polymer in poly(ethylene terephthalate) (PET)/alumina nanoparticle composites. PET is an ideal matrix for crystallization studies because the crystallinity can be controlled from nearly amorphous to highly crystalline by changing the cooling rate. In addition, the mechanical, electrical, and other physical properties of PET strongly depend on its crystallinity and crystal morphology.[16,17] For example, we recently reported a 45% increase in the wear resistance of a PET composite with 2 wt % alumina nanoparticles.[18] The incorporation of rigid inorganic nanofillers is also a promising approach for improving both the stiffness and toughness of plastics simultaneously.[6] Most research, however, has focused on PET-based nanocomposites containing clay,[8] mica,[9] fiber,[10] or submicron *and/or* macroscopic spherical particles[19] with large planar

Correspondence to: L. S. Schadler (schadl@rpi.edu) or H. Yang (yangh3@rpi.edu).
**Present address:* Intel Corporation, 5000 W Chandler Blvd, Chandler, Arizona 85226.

Contract grant sponsor: Nanoscale Science and Engineering Initiative of the National Science Foundation (NSF); contract grant number: DMR-0117792.
Contract grant sponsor: Albany International.
Contract grant sponsor: Mettler-Toledo Thermal Analysis Educational Grant 2001.

surfaces. Herein, we report the effect of hydrophilic alumina nanoparticles with high surface curvature on the crystal nucleation and growth of PET in the nanocomposites, using differential scanning calorimetry (DSC), transmission electron microscopy (TEM), and X-ray analyses.

EXPERIMENTAL

Materials

Inorganic nanoparticles tend to possess high surface energies, which often cause micron-size aggregates of the nanoparticles to form in a polymer matrix.[20–22] Hence, most previous studies in the literature exploring the effect of nanoparticles on polymer crystallization have utilized nanoparticles with functionalized surfaces that prevent their agglomeration.[23,24] However, modifying the nanoparticle surface also affects the mobility of the polymer chains in contact with them and, hence, their crystallization behavior. In this study, we have dispersed unmodified alumina nanoparticles in PET through a melt-mixing route.

PET pellets (Crystar 3939, molecular weight = $\sim$ 50,000 g/mol) were obtained from DuPont, and alumina (α-Al_2O_3) nanoparticles with an average diameter of 38 nm were obtained from Nanophase Technologies. The nanofiller surface curvature is comparable to the radius of gyration, R_g, of the PET (e.g., $R_g \sim 13$ nm for $\sim$ 85,000 g/mol).[25] The PET pellets were dried at 120°C in vacuum for 24 h and the nanoparticles were dried at 195°C in vacuum for 24 h prior to processing. The pellets and the nanoparticles were melt-blended at 260°C for 10 min at a screw speed of 80 rpm in a Thermo-Haake Polydrive Mixer. The nanofiller content was varied between 0 and 10 wt %. Finally, samples were fabricated by compression molding from the pelletized premixture at 280°C under an argon atmosphere, and cooled at a constant rate. A custom built setup was used to control the cooling rate of the mold in a press.

Characterization

To observe the nonisothermal crystallization of PET and the nanocomposites as a function of Al_2O_3 content, DSC (Mettler Toledo DSC 822e) was performed at different cooling rates: specifically, 4, 12, and 16°C/min. The peak and onset temperatures of PET crystallization were measured. To observe the subsequent melting behavior, melt-crystallized samples were heated at a constant rate of 10°C/min. The weight-fraction crystallinity ($X_c = \Delta H_{Tm}/\Delta H^o_{Tm}$) of PET in the nanocomposites was calculated from the ratio of heat of fusion in the DSC measured samples to that ($\Delta H^o_{Tm} = 140$ J/g) in theoretically 100% PET crystal.[26,27]

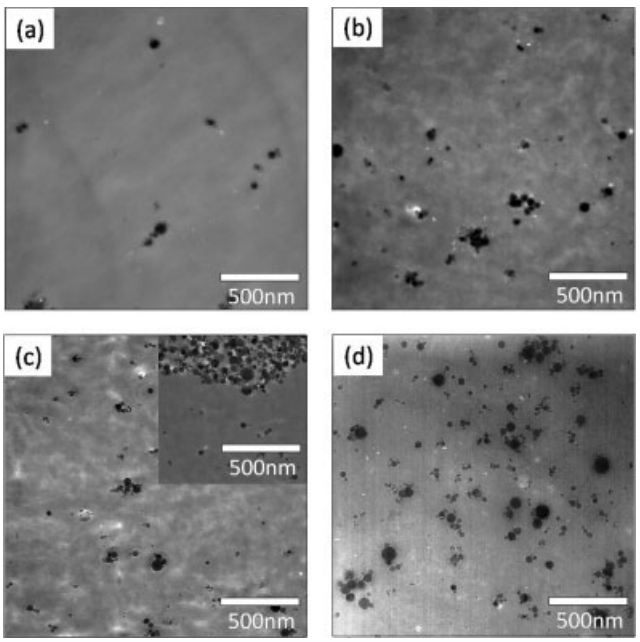

Figure 1 TEM micrographs showing the dispersion state of Al_2O_3 nanoparticles in PET matrix in (a) 1 wt %, (b) 2 wt %, (c) 5 wt %, and (d) 10 wt % Al_2O_3 filled nanocomposites.

TEM was performed using a JEOL CM-12, operating at an accelerating voltage of 120 kV. The samples melt-crystallized with a cooling rate of 16°C/min were cut to a thickness of $\sim$ 50 nm using an ultramicrotome system (MT-XL, Boeckeler Instruments) with a diamond knife (DiATOME). Then, the sectioned films were picked up on 300-mesh copper grids. In particular, to observe the PET crystalline microstructure, the films were stained with a 0.5 wt % aqueous ruthenium tetraoxide (RuO_4) solution (Electron Microscopy Sciences) for 20 min. Figure 1 represents the nanoparticle dispersion observed through TEM. The interparticle spacing (l) and the PET lamellar thickness in the samples were calculated from both TEM and small-angle X-ray scattering data. Small- and wide-angle X-ray analyses were performed at the X21 beam line of the Brookhaven National Light Source.[28]

RESULTS

Nanoparticle dispersion

One of the keys to understanding the effect of nanoparticles on polymer crystallization is to characterize the dispersion of the nanoparticles, because as the particles agglomerate both the effective particle size and l increase, which could affect both nucleation

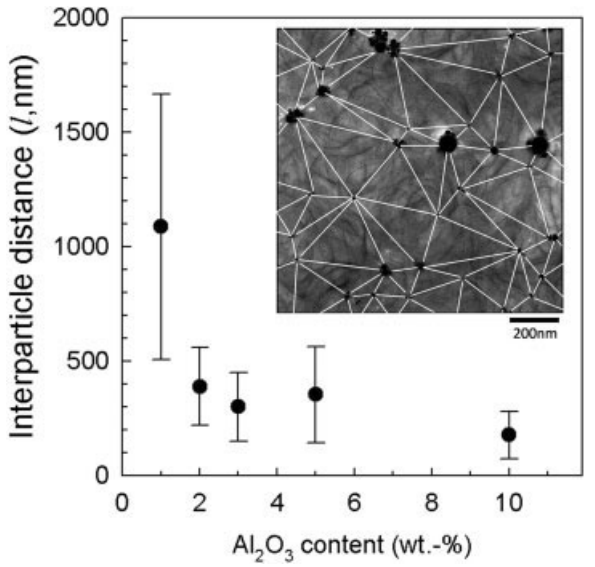

Figure 2 Variation in interparticle distance (l) distribution with nanoparticle loadings. (The inset represents an example for measuring l in a 2 wt % Al_2O_3 filled nanocomposite.)

and growth of the polymer. Figure 1 shows TEM micrographs of the nanoparticle dispersion at 1, 2, 5, and 10 wt % of the filler. At 1 wt % Al_2O_3, the particles were well dispersed in the matrix, and the average particle size was close to the reported 38 nm. At 5 wt % Al_2O_3, a few agglomerates were observed [inset in Fig. 1(c)]. At 10 wt % Al_2O_3, aggregates ranging in size from 0.3 to 1.0 μm were present. Figure 1(d) also illustrates the size distribution (10–90 nm) of the Al_2O_3 filler with average particle size of $\sim$ 38 nm. The change of l in the nanocomposites as a function of the nanoparticle content is shown in Figure 2. The value of l decreased rapidly between 1 and 3 wt % of the filler and then leveled off due to particle agglomeration.

Effect of nanoparticles on crystal nucleation

To observe the effects of dispersed nanoparticles on PET crystallization in PET/Al_2O_3 nanocomposites, the samples were nonisothermally crystallized from the melts at different cooling rates. Specifically, crystallization onset (T_{onset}) and peak (T_{peak}) temperatures were measured to study nanoparticle effects on the crystalline nucleation. Figure 3 shows typical DSC cooling curves for samples crystallized from 280°C with a cooling rate of 4, 12, and 16°C/min, respectively. T_{onset} and T_{peak} values for each DSC cooling rate are plotted against the filler content in Figure 4. The effect of cooling rate was similar for all nanoparticle loadings. The faster the cooling rate, the lower T_{peak} and the broader the crystallization peak. At 4°C/min cooling rate, T_{onset} decreased at low loadings of nanoparticles up to 3 wt % [Fig. 4(a)]. The shift in onset of crystallization to lower temperatures indicates that a greater undercooling is required to initiate polymer crystallization at lower filler loadings. However, at higher filler loadings, T_{onset} increased and was higher than that for pure PET. The same trend was observed at 12 and 16°C/min. X_c values, calculated from ΔH_{Tm} in the DSC heating curve of the sample crystallized from the melt with a cooling rate of 16°C/min, are summarized in Table I. X_c of PET in the nanocomposite decreased monotonically with an increase in Al_2O_3 content and was about 0.21 in the 5 wt % filler-loaded sample.

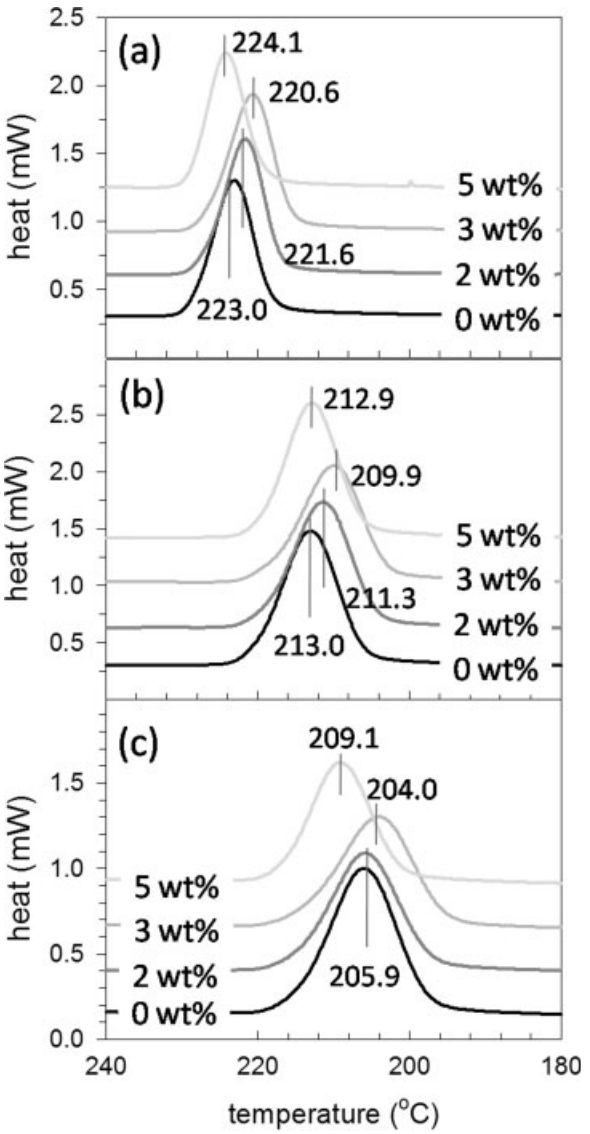

Figure 3 Effect of nanoparticle loading on PET melting curves at (a) 4°C/min, (b) 12°C/min, and (c) 16°C/min cooling rates from the melt.

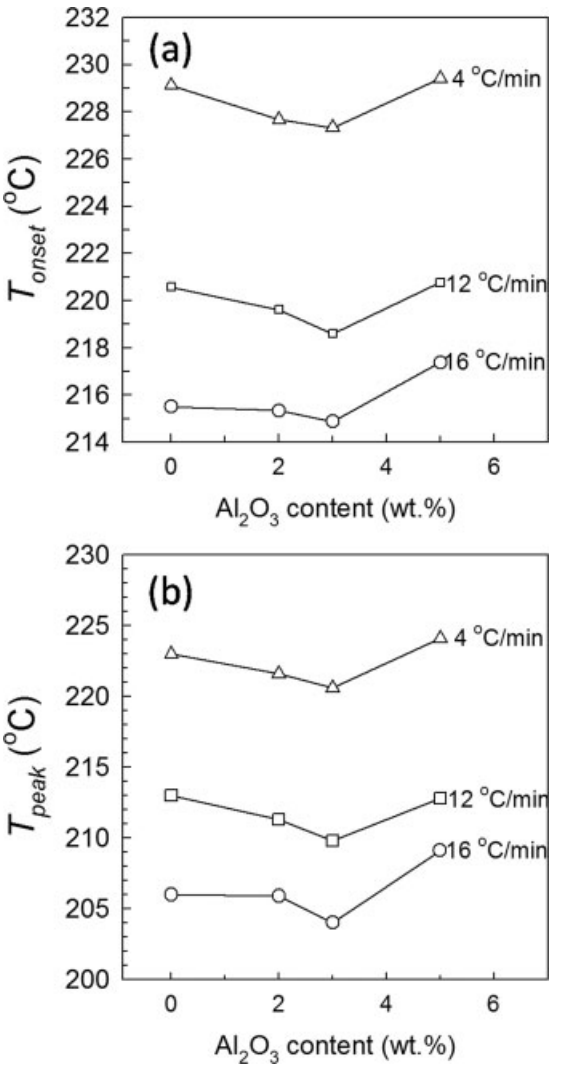

Figure 4 Variation in (a) T_{onset} and (b) T_{peak} of crystallization with filler content at 4°C/min, 12°C/min, and 16°C/min cooling rates from the melt.

The relative degree of crystallinity $X(T)$, as a function of crystallization temperature T, can be formulated as[29]

$$X(T) = \int_{T_o}^{T} \left(\frac{dH_c}{dT}\right) dT \Big/ \int_{T_o}^{T_\infty} \left(\frac{dH_c}{dT}\right) dT \qquad (1)$$

TABLE I
Characteristics of PET and PET Nanocomposites Crystallized from the Melts with a Cooling Rate of 16°C/min

	T_{peak} (°C)	T_m (°C)	X_c	q^* (nm^{-1})	D_{ave} (nm)
PET	206.1	256.1	0.275	0.483	13.0
2 wt % Al_2O_3	205.9	255.7	0.253	0.519	12.1
3 wt % Al_2O_3	204.0	255.1	0.231	0.536	11.7
5 wt % Al_2O_3	209.0	255.6	0.205	0.543	11.6

where T_o and T_∞ represent the crystallization onset and end temperatures, respectively, and dH_c is the enthalpy of crystallization released during an infinitesimal temperature range dT.

Figure 5 shows $X(T)$ as a function of T for pure PET and PET nanocomposites at various cooling rates. For a given cooling rate, the crystallization rate

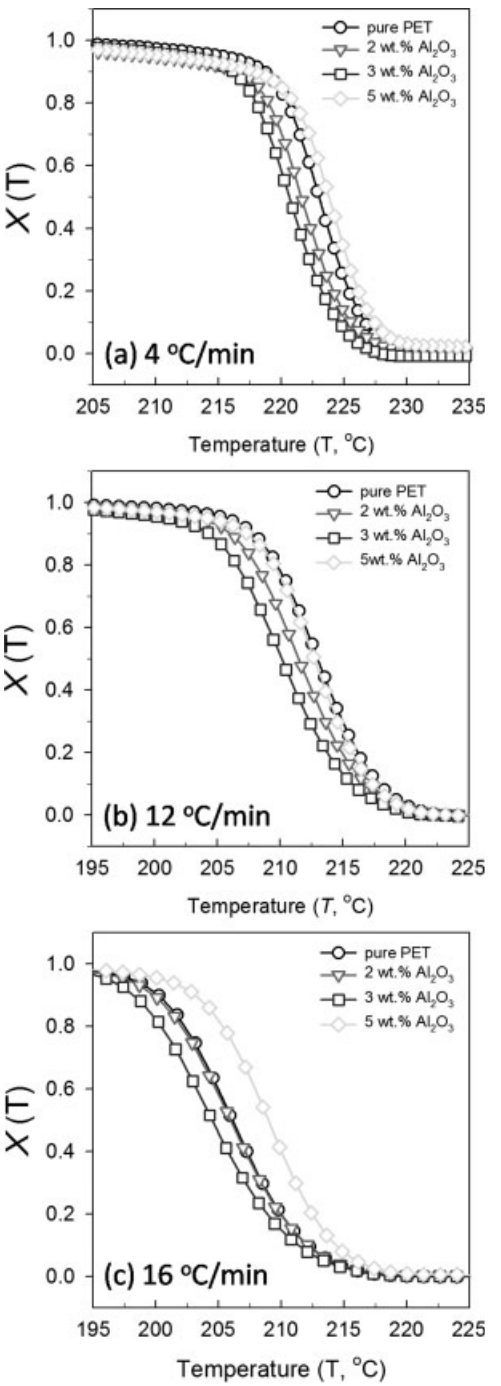

Figure 5 $X(T)$ as a function of temperature (T) for crystallization of pure PET and PET nanocomposites at different cooling rates: (a) 4°C/min; (b) 12°C/min; and (c) 16°C/min.

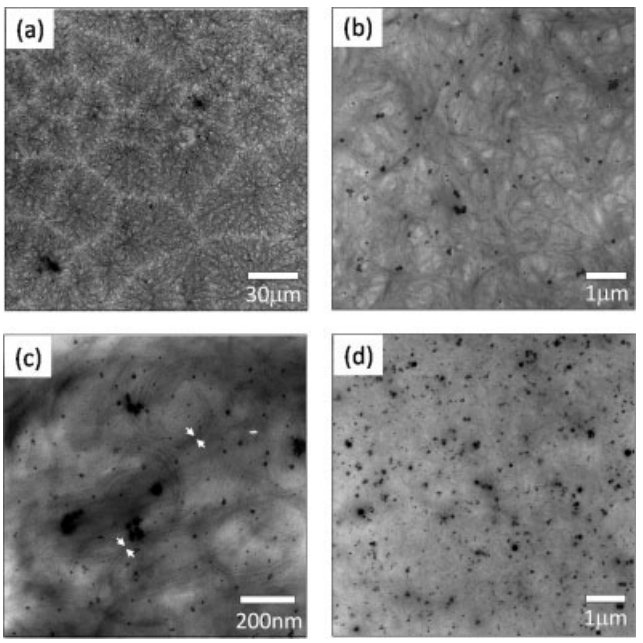

Figure 6 Effect of nanoparticle loading on spherulitic and lamellar structures in PET matrix: (a) 0 wt %, (b,c) 2 wt %, and (d) 5 wt % Al_2O_3 filled nanocomposites.

of PET nanocomposites, except for one sample containing 5 wt % Al_2O_3, decreases with an increase in Al_2O_3 content, resulting in slower crystallization of PET when compared with that of pure PET.

Effect of nanoparticles on crystalline and supramolecular structure

Figure 6 shows TEM micrographs, that clearly display the macro-and micro-crystalline morphologies in pure PET, and in 2 wt %, and 5 wt % Al_2O_3 nanocomposites, upon cooling at 16°C/min. Pure PET showed typical three-dimensional (3D) spherulites, 20–40 μm in diameter, with randomly distributed crystalline lamellae. On the contrary, the spherulitic morphology of the PET matrix was not present in either the 2 or 5 wt % Al_2O_3-filled nanocomposites. This may be because of the small interparticle spacings ($l < 350$ nm) confining the polymer chains. For example, the average lamellar thickness of PET in the 2 wt % nanocomposite, as determined from TEM images [e.g., white-arrows marked in Fig. 6(c)], was 9.1 ± 1.6 nm, lower than that (10.5 ± 1.5 nm) in pure PET.

Since lower crystallinity in the nanocomposites can induce excessive staining of the PET matrix in TEM measurement, SAXS was performed to determine the average lamellar thickness in pure PET and the PET nanocomposites. Figure 7 illustrates SAXS profiles of pure PET and the nanocomposites showing a peak shift in the scattering vector (q^*) as a function of the nanofiller loading. It is well known that a Gaussian-type scattering in SAXS profiles indicates inhomogeneous scattering neighboring centers with an average distance ($D_{ave} = 2\pi/q^*$), i.e., lamellar thickness for a semicrystalline polymer.[30] The q^* shifts to higher values on addition of nanoparticles and the average lamellar thickness (D_{ave}) decreases from 13.0 to 11.7 nm. Furthermore, in the 2 wt % Al_2O_3 nanocomposite with highly confined matrix ligament regions (i.e., $l \approx 350$ nm), the lamellae grew into ''sheaf-like'' crystallites [Fig. 6(c)], where the lamellae were curled around the alumina nanoparticles. Contrary to previous observations in the literature,[15] there is no evidence of highly-dense heterogeneous lamellae grown at the particle–matrix interface below a critical l. For the 5 wt % Al_2O_3 nanocomposites with similar l to the 2 wt % Al_2O_3 nanocomposite, we also found that most PET lamellae were randomly oriented as indicated by Figure 6(d), even though the image did not clearly show the lamellar orientation because the crystals degraded rapidly in the electron beam.

To observe any change in the crystalline structure of PET due to nanoparticle loading, XRD was performed for pure PET and the nanocomposites that were melt-crystallized with 12°C/min cooling rate. 2D XRD patterns of the samples showed typical ring patterns of the bulk crystals, irrespective of the nanoparticle loading. Figure 8 shows 1D XRD profiles obtained through circular averaging of 2D XRD patterns. In all samples, the main reflection peaks of PET crystals were at ~ 2θ = 16.1, 17.4, 21.6, 22.9, and 27.0°, corresponding to the $(0\bar{1}1), (010), (\bar{1}11), (1\bar{1}0)$ and (100) planes, respectively, of the bulk crystals with a triclinic unit cell.[21] This suggests that the dispersed nanoparticles did not affect the unit cell crys-

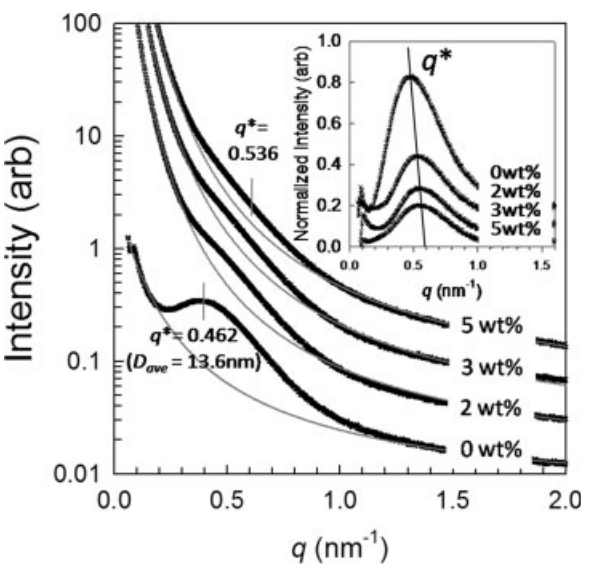

Figure 7 SAXS profiles showing effect of nanoparticle loading on PET lamellar thickness.

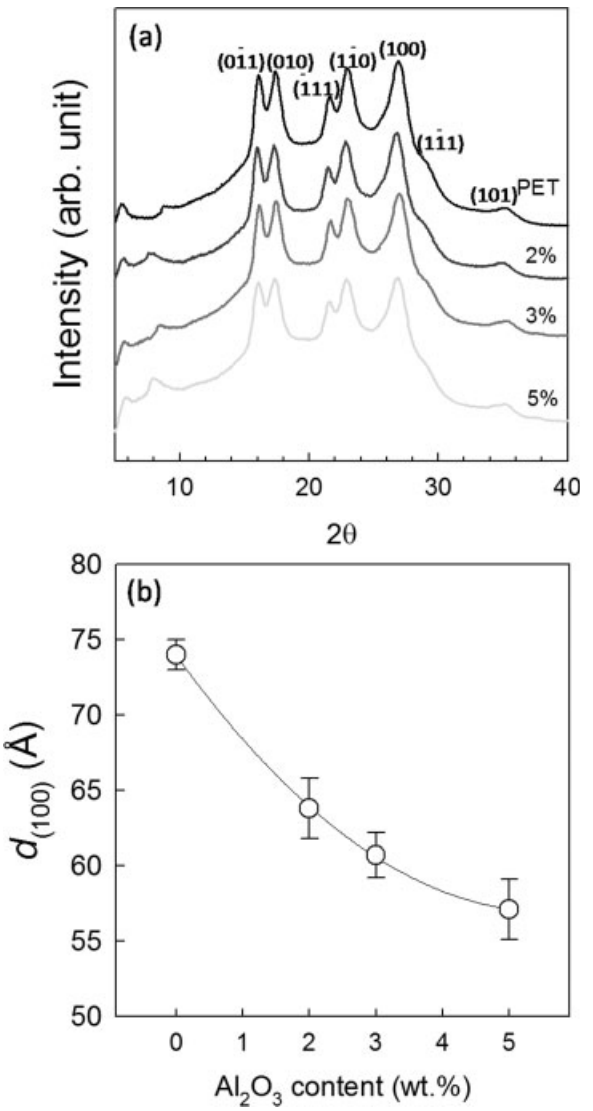

Figure 8 Effect of nanofiller content on crystalline structure of the PET matrix: (a) wide angle X-ray diffraction profiles; (b) $d_{(100)}$ in PET crystallites calculated from full-width at half-maximum (FWHM) of the (100) reflection in (a).

talline structure of PET. The XRD results also show that the diffraction peaks broadened with nanoparticle loading.

The coherence length, $d_{(hkl)}$, indicating the long-range order of the crystal planes along a *hkl* crystal direction was calculated. Because the peaks [except for the (100) reflection] overlapped with their neighboring peaks, $d_{(100)}$ was calculated using the following equation[31]:

$$d_{(100)} = \frac{57.3\lambda}{(\beta \cos \theta)} \quad (2)$$

where $\beta = (B^2 - b_o^2)^{1/2}$, B is the measured full-width (in degrees) at half-maximum (FWHM), b_o is the instrumental resolution (in degrees), λ is the wavelength of the X-radiation, and 2θ is the scattering angle at the maximum of the (100) reflection peak.

Figure 8(b) shows the coherence length $d_{(100)}$ of PET crystals in the samples as a function of the nanoparticle loading obtained from the X-ray profiles shown in Figure 8(a). The nanocomposites exhibited lower values of $d_{(100)}$, than did pure PET (74.0 ± 1.5 Å), continuously decreasing with increasing nanoparticle loading.

DISCUSSION

The results indicate that the addition of alumina nanoparticles to PET with no particular chemical bonding between the particles and the matrix does not cause heterogeneous PET crystal nucleation, if the particles are not aggregated. Specifically, TEM and DSC results suggest that there exists a sufficiently large particle size in comparison to the polymer radius of gyration necessary to induce heterogeneous nucleation from the polymer melt on the particle–matrix interface. The results also suggest that matrix confinement by the dispersed particles hinders crystal growth of PET.

Usually, the presence of a foreign surface results in crystallization occurring at lower undercoolings than in the pure polymer because of reductions in the critical nucleus size and the free energy barrier for crystallization. This is generally true if the surface is planar and the interfacial energy is relatively low. In our case, however, since the lamellar thickness typically ranges from 10 to 15 nm and is thus comparable to the size of the nanoparticles, the filler surface is no longer planar relative to the seed crystal size. Previous theoretical work has shown that a curved surface can be a poor nucleating agent compared with a planar surface.[11] If the surface curvature is high and the affinity of the crystal phase for the surface is poor, the free energy barrier is similar to the free energy barrier for homogeneous nucleation. It has also been shown previously that the nucleation rate on a curved surface is lower than the nucleation rate for homogeneous nucleation.[32] It is not clear from these studies if a curved surface will, as a rule, lead to crystallization at smaller undercoolings, even if the surface of the filler is compatible. Results with our system indicate that the presence of the alumina nanoparticles does not cause PET to heterogeneously nucleate at low alumina loadings. This is further substantiated by direct observation of the crystal morphology in the nanocomposites [Fig. 6(c)]. TEM images of the lamellar structure in the nanocomposites show that the PET lamellae do not grow from the nanoparticle surfaces. The crystal nuclea-

tion predominantly occurs in the matrix. In addition, under a confined matrix geometry such that $l < 350$ nm, the lamellae were curled around the particles and grew into a ''sheaf-like'' crystallite, which can be referred to as an incipient spherulite.

In contrast, in 5 wt % composites with Al_2O_3 aggregates ranging in size from 0.3 to 1.0 μm, T_{onset} and crystallization rate increased, suggesting that larger aggregates act like traditional micro-fillers to cause heterogeneous crystal nucleation in PET melts.

The growth of the PET crystals and formation of spherulites were also affected by the nanoparticles. Based on DSC analysis, the weight-fraction crystallinity of PET in the nanocomposites, crystallized from the melts with a cooling rate of 16°C/min, decreased to as low as 0.205 in comparison with 0.275 in pure PET. Previous studies in the literature have shown that the addition of nanoparticles can alter or induce a new crystal structure in the matrix polymer. Diffraction patterns from the nanocomposites in our study do not reveal the presence of new peaks. However, the diffraction peaks are observed to broaden with increasing filler content. The broadening of diffraction peaks is mainly related to the less-ordered crystalline structure of PET based on DSC and SAXS results. The coherence length was calculated from the FWHM of X-ray diffraction peaks using Scherrer's formula.

The calculated $d_{(100)}$ of PET crystals in PET nanocomposites are shown in Figure 8(b) as a function of Al_2O_3 loading. These results suggest that geometrical confinement by nanofiller loading interferes with the crystal growth and development of PET.

For typical bulk PET crystallites, the (100) planes tend to be stacked along a lamellar growth direction.[33] Therefore, the coherence length of either (001) or (010) planes is potentially related to a change in lamellar thickness. Since coherence lengths have linear relationships with both crystallinity and crystal perfection, the observed decreases in crystallinity and lamellar thickness of PET in the nanocomposites are consistent with a decrease in $d_{(100)}$.

Waddon and Petrovic[14] have shown that the addition of silica nanoparticles to poly(ethylene oxide) (PEO) retards the spherulitic growth rate of PEO because of matrix confinement and by pinning at the interface. We observe from Figure 6(a) that the minimum spherulite size for pure PET is $\sim$ 20 μm. Furthermore, from Figure 2, at 1 wt % loading of the nanoparticles, the interparticle distance ranges from 0.5 to 1.7 μm and at 2 wt % loading, this distance reduces to a range of 0.2–0.5 μm. Generally, filler surfaces act as heterogeneous nucleation sites, from which lamellae grow until they impinge on spherulites from neighboring particles, resulting in a large number of small spherulites. However, in the current work, the nanoparticle surfaces do not act as heterogeneous nucleation sites as long as they do not aggregate forming larger particles. This is further substantiated by direct observation of the crystal morphology in the nanocomposites. From the TEM images, it is seen that the PET lamellae do not grow from the nanoparticles and the estimated nucleation points do not coincide with the nanoparticle surfaces. The nucleation predominantly occurs in the matrix and the growth of these spherulites is impeded by the presence of the nanoparticles. Hence a disrupted spherulitic structure has been observed for the nanocomposites.

CONCLUSIONS

In this article, we have studied the effect of Al_2O_3 nanoparticles with an average diameter of 38 nm on different aspects of polymer (PET) crystal morphology. Based on the results observed, we conclude the following:

1. The nanoparticles do not act as heterogeneous nucleation sites despite their high surface energy. This is because the nanoparticles, due to their small size, cannot offer a planar surface necessary for the nucleation of the polymer crystals.
2. The addition of the nanoparticles disrupts the spherulitic morphology in the polymer matrix because of their physical presence and their proximity to one another.
3. The lamella thickness is observed to decrease with increasing filler content. This result is consistent with an observed decrease in $d_{(100)}$ in the nanocomposites.
4. X-ray diffraction patterns for the nanocomposites do not show additional peaks compared with those observed for pure PET, indicating that the unit cell structure is not affected by the incorporation of the nanoparticles.

References

1. Keller, A. J Polym Sci 1955, 17, 291.
2. Strobl, G. Eur Phys J E 2000, 3, 165.
3. Stein, R. S.; Misra, A. J Polym Sci Polym Phys Ed 1973, 11, 109.
4. Shi, H. F.; Zhao, Y.; Dong, X.; He, C. C.; Wang, D. J.; Xu, D. F. Polym Int 2004, 53, 1672.
5. Wang, C.; Hwang, L. M. J Polym Sci Part B: Polym Phys 1996, 34, 1435.
6. Chan, C. M.; Wu, J. S.; Li, J. X.; Cheung, Y. K. Polymer 2002, 43, 2981.
7. Liu, W. T.; Tian, X. Y.; Cui, P.; Li, Y.; Zheng, K.; Yang, Y. J Appl Polym Sci 2004, 91, 1229.
8. Wan, T.; Chen, L.; Chua, Y. C.; Lu, X. H. J Appl Polym Sci 2004, 94, 1381.
9. Okamoto, M.; Shinoda, Y.; Okuyama, T.; Yamaguchi, A.; Sekura, T. J Mater Sci Lett 1996, 15, 1178.

10. Beaudoin, O.; Bergeret, A.; Quantin, J. C.; Crespy, A. Polym Compos 2002, 23, 87.
11. Lee, J. K.; Choy, J. H.; Choi, Y. Surf Sci 1991, 256, 147.
12. Turturro, G.; Brown, G. R.; Stpierre, L. E. Polymer 1984, 25, 659.
13. Kim, S. H.; Ahn, S. H.; Hirai, T. Polymer 2003, 44, 5625.
14. Waddon, A. J.; Petrovic, Z. S. Polym J 2002, 34, 876.
15. Bartczak, Z.; Argon, A. S.; Cohen, R. E.; Kowalewski, T. Polymer 1999, 40, 2367.
16. Asano, T.; Calleja, F. J. B.; Flores, A.; Tanigaki, M.; Mina, M. F.; Sawatari, C.; Itagaki, H.; Takahashi, H.; Hatta, I. Polymer 1999, 40, 6475.
17. Yamada, Y.; Tanaka, K. Wear 1986, 111, 63.
18. Bhimaraj, P.; Burris, D. L.; Action, J.; Sawyer, W. G.; Toney, C. G.; Siegel, R. W.; Schadler, L. S. Wear 2005, 258, 1437.
19. Groeninc, G.; Berghman, H.; Overberg, N.; Smets, G. J Polym Sci Polym Phys Ed; 1974, 12, 303.
20. Garcia, M.; Garcia-Turiel, J.; Norder, B.; Chavez, F.; Kooi, B. J.; van Zyl, W. E.; Verweij, H.; Blank, D. H. A. Adv Eng Mater 2004, 6, 724.
21. Kuo, S. L.; Chen, Y. C.; Ger, M. D.; Hwu, W. H. Mater Chem Phys 2004, 86, 5.
22. Rong, M. Z.; Zhang, M. Q.; Pan, S. L.; Lehmann, B.; Friedrich, K. Polym Int 2004, 53, 176.
23. Ma, D. L.; Hugener, T. A.; Siegel, R. W.; Christerson, A.; Martensson, E.; Onneby, C.; Schadler, L. S. Nanotechnology 2005, 16, 724.
24. Du, S. G.; Yan, J.; Zhang, T. L.; Cui, H. P.; Liu, J. Z. Key Eng Mater 2005, 280–283, 1033.
25. Mcalea, K. P.; Schultz, J. M.; Gardner, K. H.; Wignall, G. D. Macromolecules 1985, 18, 447.
26. Chen, H. L.; Hwang, J. C. Polymer 1995, 36, 4355.
27. Qiu, G.; Tang, Z. L.; Huang, N. X.; Gerking, L. J Appl Polym Sci 1998, 69, 729.
28. Yang, H. C.; Shin, T. J.; Ling, M. M.; Cho, K.; Ryu, C. Y.; Bao, Z. N. J Am Chem Soc 2005, 127, 11542.
29. Cebe, P.; Hong, S. D. Polymer 1986, 27, 1183.
30. Strobl, G. R.; Muller, N. J Polym Sci Polym Phys Ed 1973, 11, 1219.
31. Mo, Z.; Lee, K. B.; Moon, Y. B.; Kobayashi, M.; Heeger, A. J.; Wudl, F. Macromolecules 1985, 18, 1972.
32. Brar, T.; France, P.; Smirniotis, P. G. J Phys Chem B 2001, 105, 5383.
33. Yang, H. C.; Bhimaraj, P.; Yang, L.; Siegel, R. W.; Schadler, L. S. J Polym Sci Part B: Polym Phys 2007, 45, 747.